

The effects of initial sol parameters on the microstructure and optical transparency of TiO₂–SiO₂ binary aerogels

J. H. LEE, S. Y. CHOI, C. E. KIM

Department of Ceramic Engineering, Yonsei University, 134 Shinchon-dong, Seoul, 120-749, Korea

G. D. KIM

Division of Ceramics, Korea Institute of Science and Technology, P.O. Box 131, Cheongryang, Seoul, Korea

The effects of initial sol parameters on the pore structure and optical transparency of TiO₂–SiO₂ binary aerogels are investigated. Different silicon alkoxides, catalysts and water to alkoxide ratios were considered as initial sol parameters to control the hydrolysis and condensation reactions in each reaction stage. Strongly acidic conditions gave rise to the most transparent monolithic aerogels for both tetra-ethyl ortho silicate (TEOS) and tetra methyl ortho silicate (TMOS) based systems. In the TMOS-based system, due to a larger number of monosilicic acids acting as equivalent nucleation centres for further growth, smaller and uniformly distributed particles and interstitial pores were produced during the gelation and supercritical drying. Therefore, with the same catalyst and water content, better transparency was observed in the TMOS-based system than in the TEOS-based system.

1. Introduction

Gels and glasses containing titanium are of considerable technological and scientific interest. Glasses in the silica–titania system show a good chemical stability, a very low thermal expansion and a high refractive index. Amongst the applications of silica–titania materials is as acting as a support material for dispersed metals and catalytically active oxides [1–3].

Because of the advantages of the sol–gel method, it has been employed to produce gels or glasses of silica–titania [4, 5] mixed oxides. However, a major problem in producing monoliths or glasses by the sol–gel route is the formation of cracks during the drying stage. In practice the xerogel method requires a considerable drying time, whereas aerogel monoliths, with the use of the supercritical drying technique, can be obtained in a few hours [6, 7].

In silica–titania binary aerogels and also silica aerogels, the amount of added water and the amount of solvent and catalyst used, have a direct influence on the hydrolysis and polycondensation behavior of the metal alkoxides used in the synthesis and hence the structure and homogeneity of the final aerogel.

A few reports have been published in the literature on silica–titania aerogels with most of them being concerned with either the processing methods or the crystallization behaviour of the aerogel [8, 9]. Only a few investigations have been performed in order to study the effect of the initial sol parameters and the

control of hydrolysis and condensation reactions, on the properties of the final aerogel.

It is the purpose of this paper to evaluate the effects of a catalyst, the amount of water added in each step of the two-step process and the length of the alkyl chain of the silicon alkoxide, on the pore structure and optical transparency of a silica–titania aerogel.

2. Experimental procedure

Tetra methyl ortho silicate, Si(OCH₃)₄, tetra ethyl ortho silicate, Si(OC₂H₅)₄ and titanium isopropoxide, Ti(OⁱC₃H₇)₄ were used as the starting materials for the preparation of gels in the TiO₂–SiO₂ system. The chemical composition of the gels were 3 mol % TiO₂ with the balance being SiO₂. Because of the large difference in the hydrolysis rates between the titanium alkoxide and the silicon alkoxide, the titanium alkoxide was chelated with AcAc (acetylacetone) and the silicon alkoxide was prehydrolysed in the 1st step of a two-step process.

To investigate the influence of the degree of hydrolysis and condensation in each step on the properties of the final aerogel, the catalysts, water contents and silica precursors were varied, as is listed in Table 1. The compositions were varied in order to optimize the homogeneity of the microstructure and transparency. HCl and NH₄OH were used as the acid and base catalysts, respectively. Fig. 1 shows

TABLE I Compositions of the starting solutions

Designation	Si alkoxide	Ti alkoxide ^a	solvent(R ^b)	H ₂ O(r ^c)	Catalyst	
					1st	2nd
E6BB1	TEOS 0.97	TIP 0.03	EtOH 4	6	base 0.01	base 0.01
E6BB2	TEOS 0.97	TIP 0.03	EtOH 4	6	base 0.001	base 0.01
E6AB	TEOS 0.97	TIP 0.03	EtOH 4	6	acid 0.01	base 0.01
E1.5AA	TEOS 0.97	TIP 0.03	EtOH 4	1.5	acid 0.01	acid 0.01
E3AA	TEOS 0.97	TIP 0.03	EtOH 4	3	acid 0.01	acid 0.01
E6AA	TEOS 0.97	TIP 0.03	EtOH 4	6	acid 0.01	acid 0.01
M6AB	TMOS 0.97	TIP 0.03	MeOH 4	6	acid 0.01	base 0.01
M6AA	TMOS 0.97	TIP 0.03	MeOH 4	6	acid 0.01	acid 0.01
M3AA1	TMOS 0.97	TIP 0.03	MeOH 4	3	acid 0.01	acid 0.01
M3AA2	TMOS 0.97	TIP 0.03	MeOH 4	3	acid 0.05	acid 0.05
M3AA3	TMOS 0.97	TIP 0.03	MeOH 4	3	acid 0.1	acid 0.1

^a all TIPs were complexed by acetylacetonone with the mole ratio of AcAc/TIP = 1

^b R = solvent/alkoxide (in mole ratio)

^c r = water/alkoxide (in mole ratio)

all numbers in this table are mole ratio

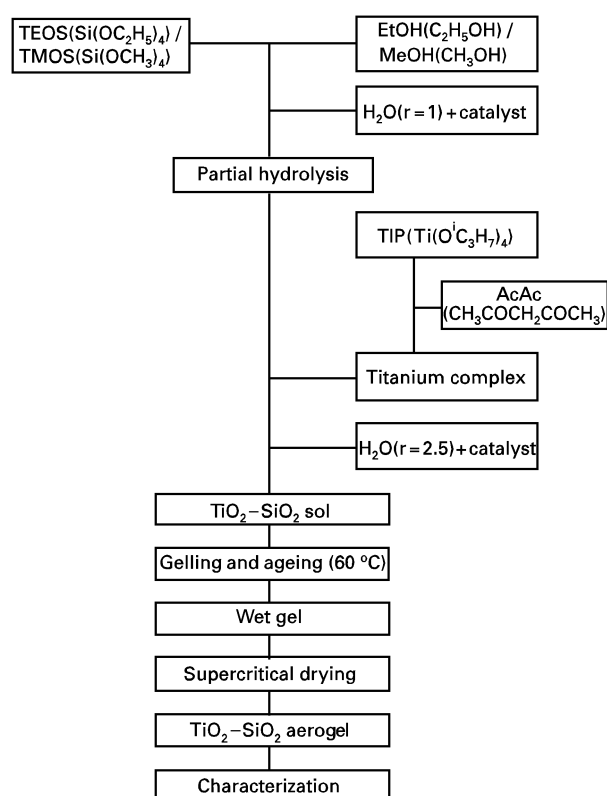


Figure 1 Schematic diagram of the experimental procedure for the preparation of the TiO₂-SiO₂ binary aerogels.

a schematic diagram of the experimental procedure. As-prepared solutions were poured into test tubes and after gelation at 60 °C, the samples were kept at the same temperature for approximately twice the gelation time for syneresis and then supercritically dried in an autoclave.

The conditions of our supercritical drying process are as follows: after insertion of the wet gels, the autoclave was filled with N₂ gas up to a pressure of 5.516 mPa, in order to diminish temperature gradients and also to suppress the boiling of the liquid. The temperature was then slowly increased above the critical temperature and pressure of either ethanol or

methanol. Then at a constant temperature of 280 °C, the solvent vapours were evacuated. When the pressure reached atmospheric pressure, the autoclave was flushed with dry N₂ in order to remove any remaining trapped solvent.

The aerogels were characterized by using an ultra violet/visible spectrum (UV/VIS) spectrometer in order to evaluate the transmittance of the aerogel. Relatively large pores (>0.1µm in diameter) were evaluated by mercury penetration porosimetry. For smaller pores (<0.01µm in diameter) nitrogen adsorption-desorption isotherms were employed. The microstructure of the aerogels was observed by scanning electron microscopy (SEM) on a fractured surface.

3. Results

3.1. The tetra ethyl ortho silicate (TEOS) based system

The gelation behaviours of the binary TiO₂-SiO₂ sols made from the TEOS-based system are summarized in Table II.

The two-step-base catalysis scheme produced precipitation, with additions of NH₄OH as small as 0.001 moles in the 1st hydrolysis step. The addition of the acid catalyst in the 1st step produced orange or yellow clear solutions. In the case of sample E6AB, a clear solution and a transparent wet gel could be obtained.

The addition of the acid catalyst to the 1st step increased the hydrolysis rate of the TEOS due to the production of monosilicic acids. The addition of the acid catalyst to the 2nd step suppressed the condensation reaction of both the silanol group and the hydrolyzed titania species (Ti(OH)_x(OR)_{3-x}(AcAc), x = 1, 2 or 3). Therefore, two-step-acid catalysis produced yellow clear solutions and transparent wet gels for all samples in which the water content ranged from 1.5–6.

The gelation time for sample E1.5AA was nearly 15 days at 60 °C and 100 days at room temperature. Accordingly we did not prepare an aerogel at this composition.

TABLE II Descriptions of binary TiO₂-SiO₂ sols and aerogels in TEOS-based systems

Sample designation	pH of sol before molding	Visual description of sol	Gelation time (60 °C, h)	Visual description of aerogel
E6BB1	9.00	Precipitate	—	—
E6BB2	7.70	Precipitate	—	—
E6AB	5.25	Orange, clear	9	Opaque
E1.5AA	1.10	Yellow, clear	> 360	Not prepared
E3AA	2.00	Yellow, clear	57	Slightly transparent
E6AA	2.09	Yellow, clear	35	Translucent

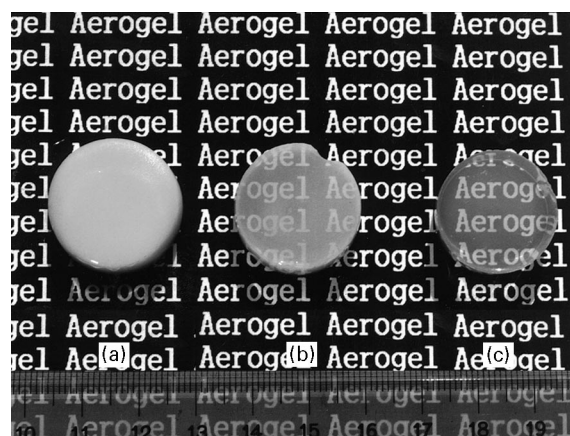


Figure 2 Photograph of the monolithic aerogels from the TEOS-based systems (All specimens are 1 cm in thickness.); (A) E6AB, (B) E6AA and (C) E3AA.

Figs. 2 and 3 show a photograph and the transmittance curve of aerogels prepared under different sol conditions. An opaque aerogel was produced by using the acid catalyst in the 1st step and the base in the 2nd step (E6AB). On the other hand, the 2-step-acid catalysed aerogel was slightly transparent or translucent. In addition a more transparent aerogel was obtained as the water ratio was decreased (E3AA).

The pore size analysis using mercury porosimetry is limited to macropores (pores larger than 0.1 μm.) [10]. Figs. 4 and 5 show the incremental intrusion volume of the opaque E6AB aerogel and the translucent E6AA aerogel measured using the mercury porosimetry technique.

The clear transparency of the monolithic aerogel gives an upper limit for the pore size of about 0.1 μm [11]. As is shown in Fig. 4, most of the total intrusion volume fills macropores for the opaque E6AB aerogel. This macroporosity explains the opacity of the E6AB aerogel. The E6AA aerogel also contains macropores but their relative amount is smaller than that of the E6AB, opaque aerogel.

The N₂ adsorption and desorption method which is applicable for pores smaller than ~0.1 μm [10], was used in the evaluation of the meso- and micropores. Figs. 6 and 7 show the N₂ adsorption-desorption isotherms for the translucent E6AA and more transparent E3AA aerogels, respectively. Both of these aerogels exhibit type-IV adsorption isotherms which is considered to indicate the presence of mesopores, i.e., pores with a width between 1.5–50 (or 100) nm [12]. The isotherms of both samples show saturation

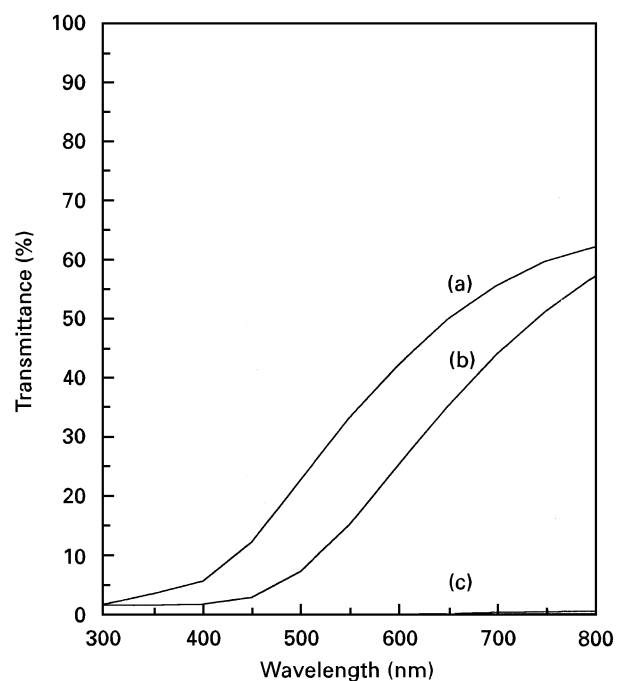


Figure 3 UV/VIS spectra for monolithic aerogels in the TEOS-based systems, (a) E3AA, (b) E6AA, (c) E6AB.

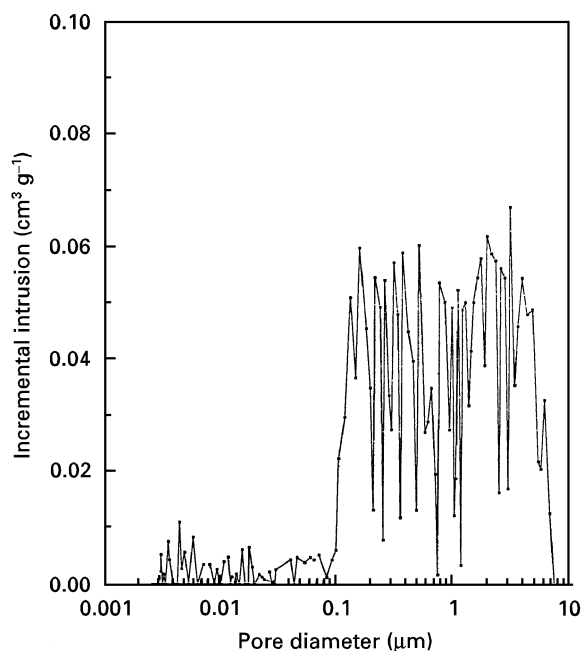


Figure 4 Incremental intrusion of E6AB aerogel measured using the Hg porosimetry technique.

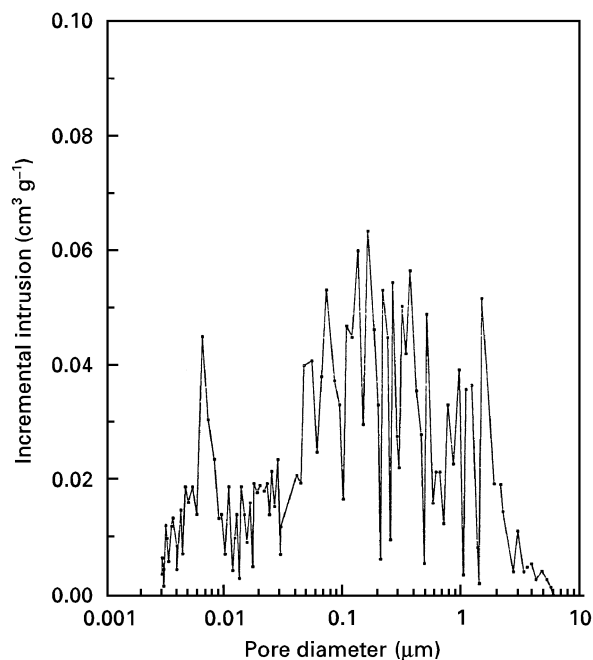


Figure 5 Incremental intrusion of E6AA aerogel measured using the Hg porosimetry technique.

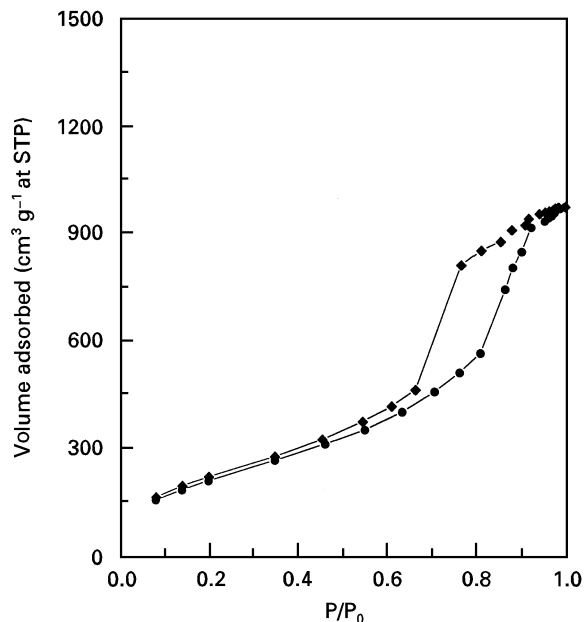


Figure 7 Nitrogen (●)adsorption-(◊)desorption isotherm for the E3AA aerogel.

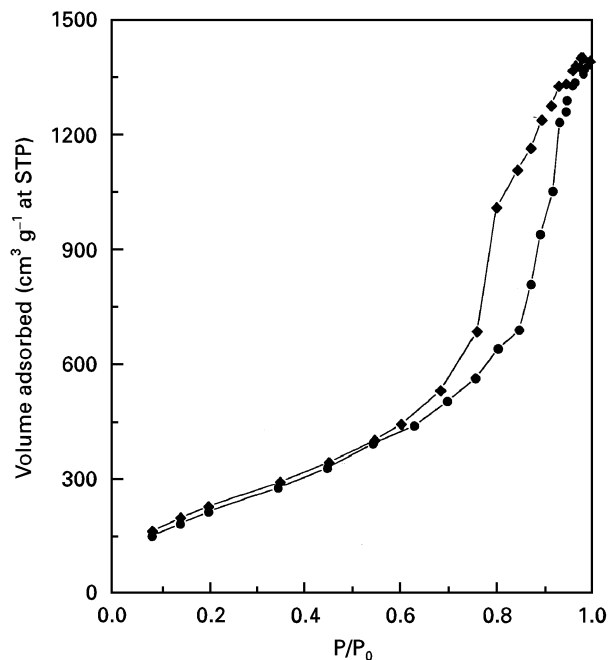


Figure 6 Nitrogen (●)adsorption-(◊)desorption isotherm for the E6AA aerogel.

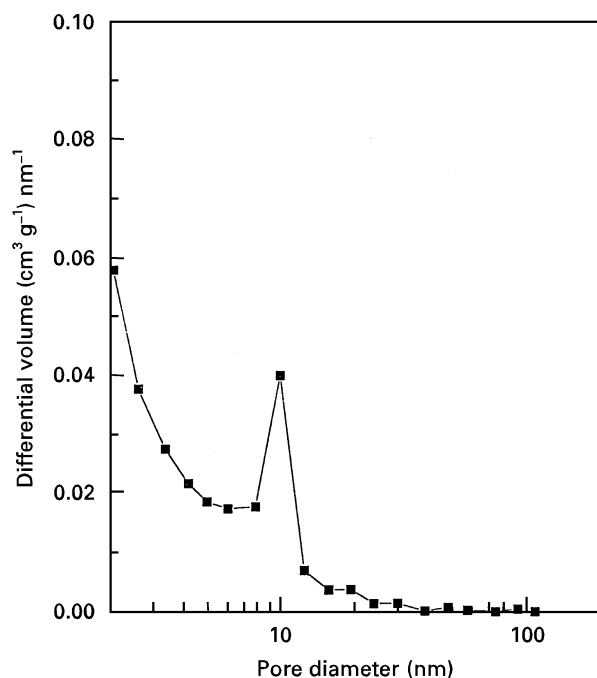


Figure 8 Differential pore volume plot for the E6AA aerogel.

effects but they are much more pronounced for the E3AA sample. For the E6AA sample, the shape of the hysteresis loop is that of type H1 of the IUPAC classification, whilst the hysteresis loop of the E3AA sample is that of type H2 [13].

The Brunauer–Emmett–Teller (BET) surface area of the E6AA and E3AA samples are 850.39 and 792.52 $\text{m}^2 \text{g}^{-1}$, respectively. We observe no direct relationship between the BET surface area and the sample transparency.

The pore-size distributions for samples E6AA and E3AA were calculated using the Pierce method [14],

and the results are shown in Figs. 8 and 9. In the aerogel prepared at the composition of E6AA, most of the pores have a size in the range of 8–10 nm. A small number of pores had a size larger than 10 nm. For the E3AA samples most of the pores had sizes in the range of 5–8 nm and it should be noted that no pores larger than 30 nm were observed. These pore-size distributions explain the observed difference in the optical transparency of the two samples.

SEM photographs of the fractured surface for the aerogels made from the TEOS-based system are shown in Fig. 10(a–c). The aerogels had a granular structure composed of spherical particles of 30–60 nm in diameter. Large interstitial pores can be observed in

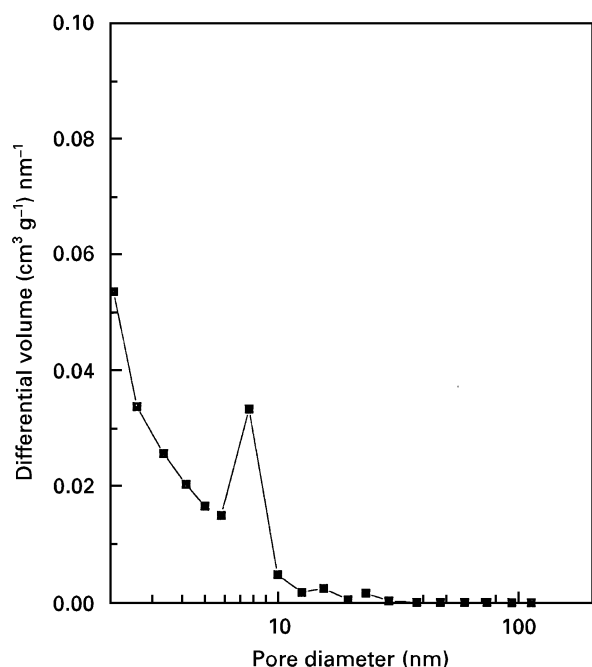


Figure 9 Differential pore volume plot for the E3AA aerogel.

the opaque E6AB aerogel whilst the pore size of the translucent or transparent E3AA aerogel is smaller and more homogeneous than that of the opaque E6AB aerogel.

3.2. Tetra-methyl ortho silicate (TMOS) based system

The gelation behaviour of the binary $\text{TiO}_2\text{-SiO}_2$ sols made from TMOS-based systems are summarized in Table III. As in the case of the TEOS-based systems, orange or yellow clear solutions and wet gels were obtained in acidic conditions. The gelation time of the M6AA sol was shorter than that of the M3AA1 sol by 11 h and the gelation times of the M3AA2 and M3AA3 sols were even shorter than that of the M6AA sol.

Therefore, we can conclude that the water content is the dominant factor which affects the gelation time in acidic conditions up to a 0.01 molar ratio. The effect of the catalyst is more pronounced than that of the water content under strong acidic conditions.

The gelation times of the TMOS-based systems were, on the whole, shorter than those of the TEOS-based systems.

Fig. 11 shows a photograph of the monolithic aerogels. As in the case of the TEOS-based system, an opaque aerogel was produced by the addition of the NH_4OH in the 2nd step. For identical catalyst and water content conditions a far more transparent aerogel was obtained in the TMOS-based system (M6AA and M3AA in Fig. 11) than in the TEOS-based system (E6AA and E3AA in Fig. 2).

Increasing the amount of the catalyst also produced clearer aerogels, as is shown by samples M3AA2 and M3AA3 in Fig. 11. However the difference in transparency between these samples is not distinguishable with the naked eye. However differences in the trans-

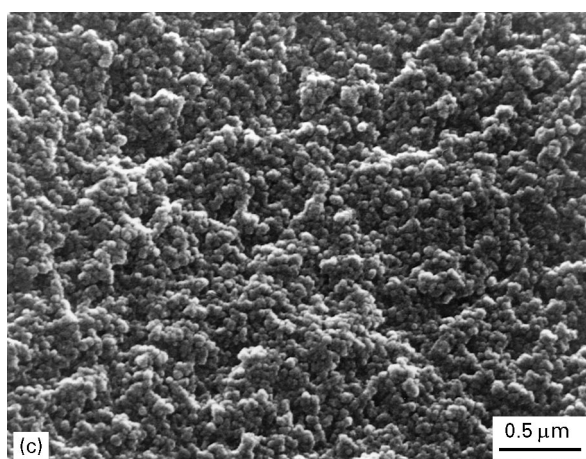
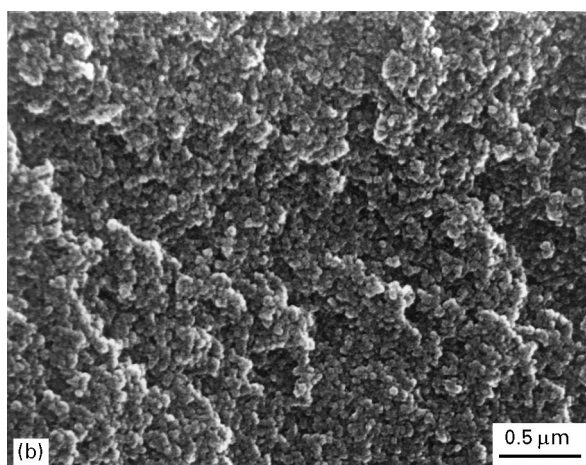
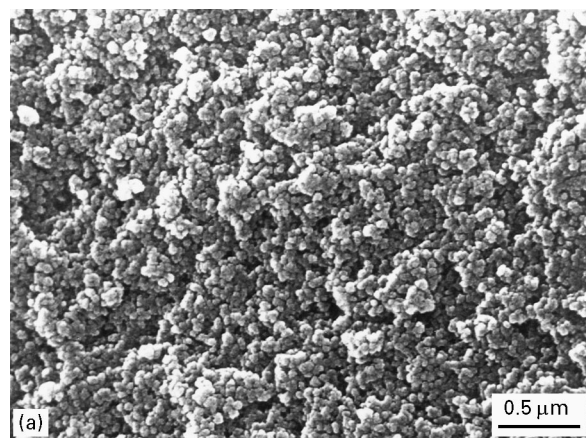


Figure 10 Scanning electron micrographs of aerogel fragments in the TEOS-based systems; (a) E6AB, (b) E6AA and (c) E3AA.

parency of the aerogels could be observed in the transmittance curves obtained using the UV/VIS spectrometer, as is shown in Fig. 12. The M3AA3 sample transmits more light at wavelengths less than 650 nm than does the M3AA1 sample and similar behaviour is observed at wavelengths longer than 650 nm. The transmittance of the M3AA2 sample is much larger than the M3AA1 or M3AA3 samples. Thus strong acidic conditions appear to produce clear aerogels with the optimum acid content being less than a 0.05 molar ratio to TMOS.

Figs. 13 and 14 show the isotherms of a mostly transparent but slightly hazy M6AA sample and a very clear M3AA2 sample. Both isotherms can be classified as type IV [12]. The shape of the hysteresis

TABLE III Descriptions of the binary TiO₂-SiO₂ sols and aerogels in the TMOS-based systems

Sample designation	pH of sol before molding	Visual description of sol	Gelation time (60 °C, h)	Visual description of aerogel
M6AB	5.62	Orange yellow, clear	0.5	Opaque
M6AA	1.45	Light yellow, clear	22	Slightly transparent
M3AA1	1.25	Light yellow, clear	33	Transparent
M3AA2	0.30	Yellow, clear	11	Transparent
M3AA3	-0.21	Yellow, clear	6	Transparent



Figure 11 Photograph of the monolithic aerogels in the TMOS-based systems (All specimens are 1 cm in thickness.); (A) M6AB, (B) M3AA1, (C) M6AA, (D) M3AA2 and (E) M3AA3.

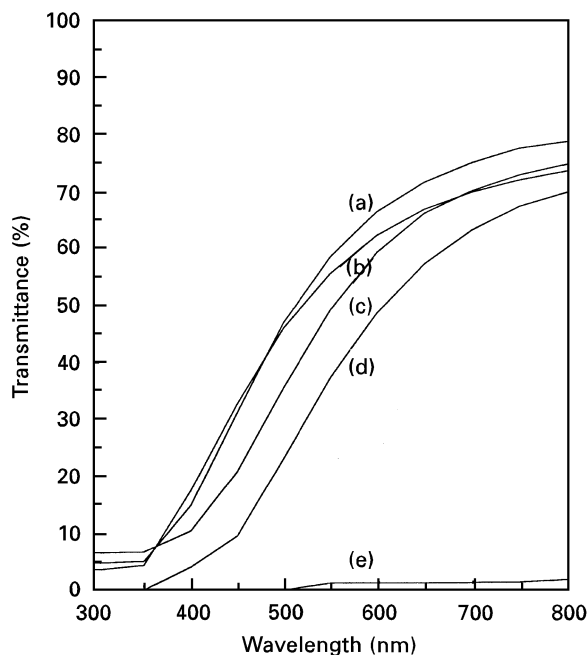


Figure 12 UV/VIS spectra for monolithic aerogels in the TMOS-based systems; (a) M3AA2, (b) M3AA3, (c) M3AA1, (d) M6AA and (e) M6AB.

loops mimics that of type H2 of the IUPAC classification [13] as in the case of the E3AA sample in the TEOS-based system. This indicates that a well-developed mesoporous structure exists in both samples.

The BET surface areas are 936.84 and 995.63 m² g⁻¹ for the M6AA and M3AA2 samples, respectively. The pore size distributions of the M6AA and M3AA2 samples are shown in Figs. 15 and 16, respectively and are in the range of 3–7 nm for both samples. However the M3AA2 sample shows a smaller pore

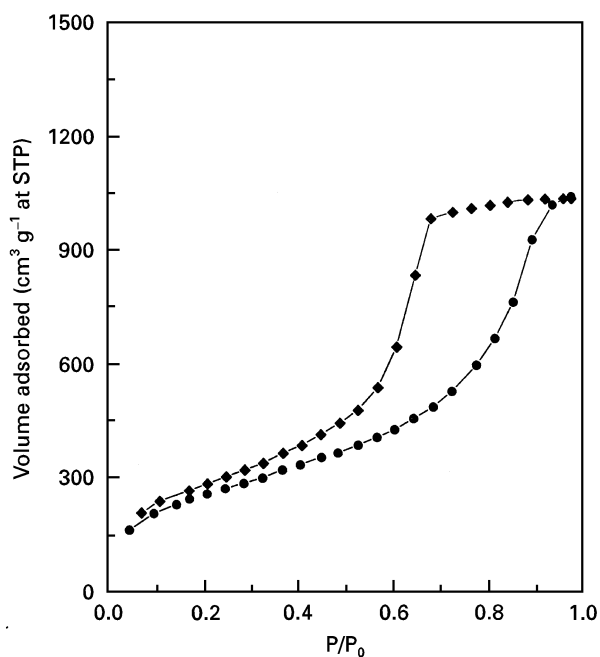


Figure 13 Nitrogen (●)adsorption-(◆)desorption isotherm for the M6AA aerogel.

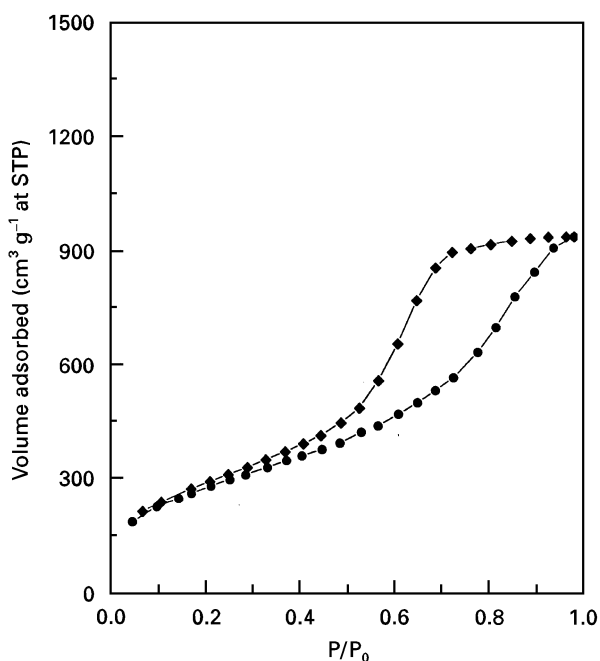


Figure 14 Nitrogen (●)adsorption-(◆)desorption isotherm for the M3AA2 aerogel.

size and unimodal maximum than does the M6AA sample. It is remarkable that these values are much smaller in size and have a narrower size distribution than those of the TEOS-based samples.

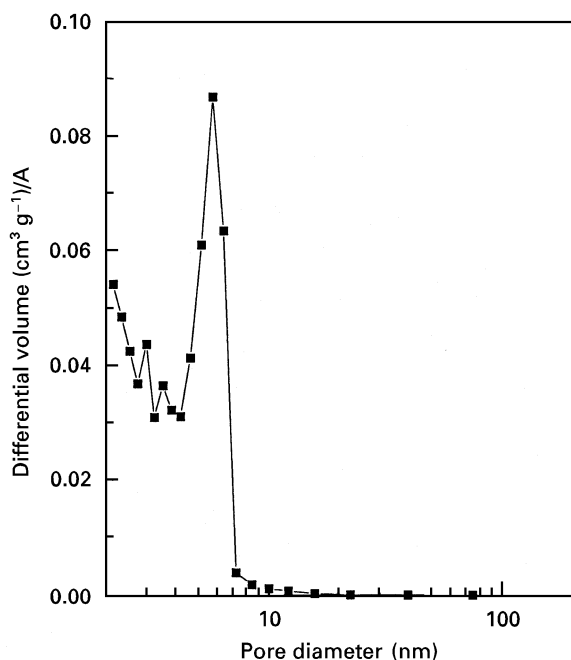


Figure 15 Differential pore volume plot for the M6AA aerogel.

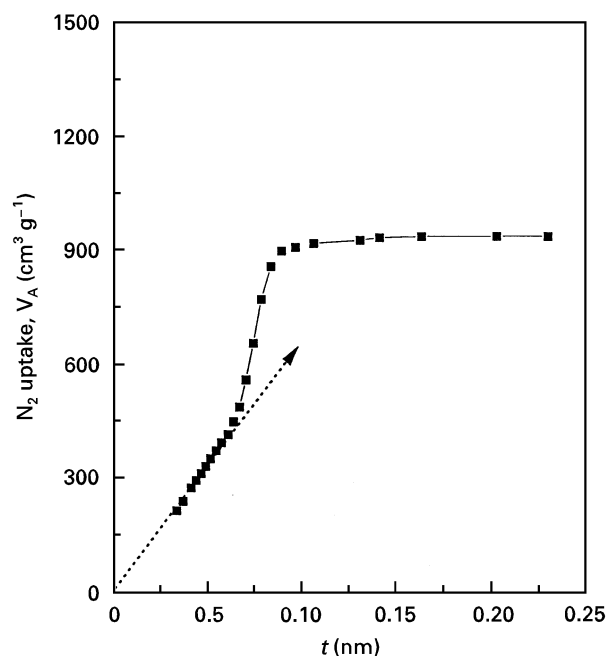


Figure 17 de Boer's t -plot character for the M3AA2 aerogel.

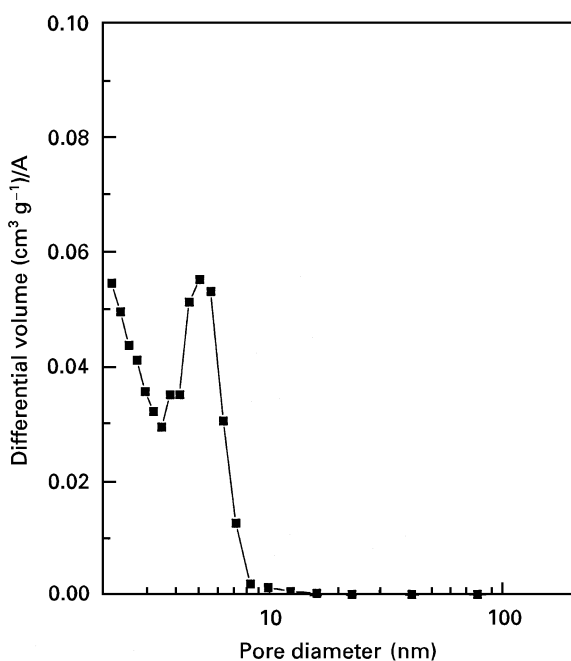


Figure 16 Differential pore volume plot for the M3AA2 aerogel.

In order to check the existence of microporosity, the t -method [13] has been applied to the M3AA2 sample and its t -plot is shown in Fig. 17. The plot can be fitted to a straight line passing through the origin. This indicates that no microporosity exists in the sample.

SEM photographs of the fractured surface for the opaque M6AB aerogel and for the most transparent M3AA2 aerogel made from the TMOS-based system are shown in Fig. 18(a and b). The aerogels had a granular structure composed of spherical particles, similar to that of the aerogels in the TEOS-based system. However the size of the spherical particles was much smaller than those observed in the TEOS-based aerogels. These aerogels have particle sizes of 15–30 nm in diameter which is about two times small-

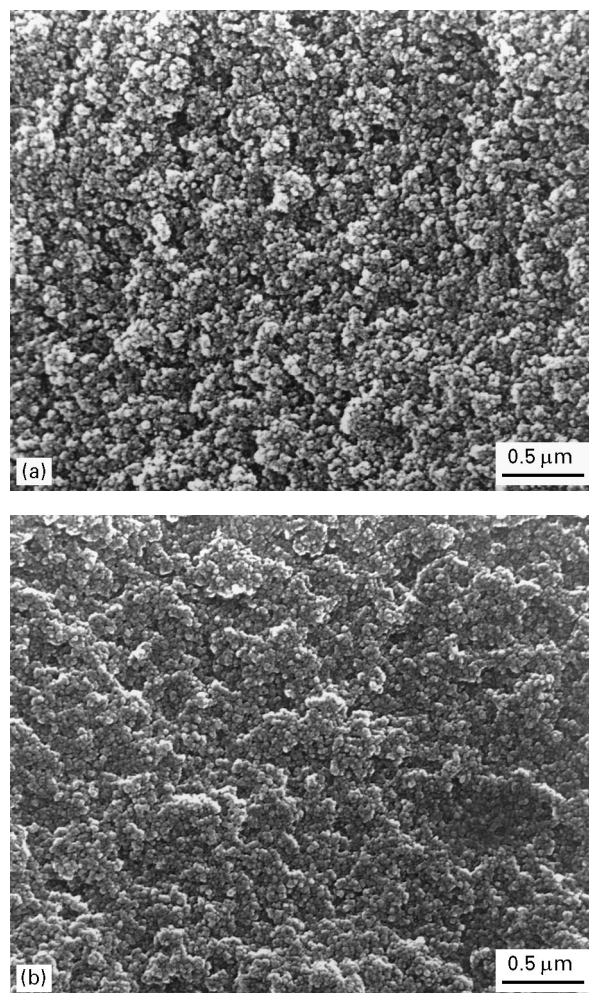


Figure 18 Scanning electron micrographs of aerogel fragments in the TMOS-based systems; (a) M6AB and (b) M3AA2.

er than the values found for the TEOS-based system. In the opaque M6AB aerogel, large pores between the solid phase could be observed. The clear and transparent M3AA2 aerogel had very small pores and

a homogeneous microstructure. Remnant samples showed intermediate microstructures between these two extreme samples. These microstructures confirmed the observed difference in optical transparency.

4. Discussion

A TiO_2 single component sol is stable only at values of the $\text{pH} < 3$ and above this value, precipitation occurs. However no precipitation is observed and thus the solution remains clear when the titanium alkoxide is stabilized with AcAc [15]. In the TiO_2 - SiO_2 binary system, strong basic conditions and a large excess of water for the titanium precursor in the 2nd step increased the hydrolysis and condensation rates, thus producing precipitation.

At the wet gel stage, all the samples that had been acid-catalysed in the 1st step were very clear and transparent for both the TEOS and TMOS-based systems. When the basic catalyst was added in the 2nd condensation step, the polycondensation reaction did not proceed as much in the wet-gel stage. Therefore, the sol was stable and the wet gel was able to remain transparent. However, the aerogel obtained at the same composition had a large amount of macropores and coarse pore structure because the high temperature and pressure during the supercritical drying accelerated the polycondensation reaction. The acid catalyst in the 2nd step however controls the condensation reaction of the silanol group and hydrolysed titania species. The reaction control is maintained under the high temperature and high pressure conditions produced during supercritical drying.

We observed differences in the microstructures and optical transparencies between TEOS and TMOS-based systems. The use of an acid catalyst in the 1st step promoted the hydrolysis rate and suppressed the condensation rate, resulting in silanol monomers rather than oligomeric silicate species [16]. In the TEOS-based system, insufficient monosilicic acid groups that act as a potential nuclei for further growth are produced, although they are catalysed by the acid in the 1st step. When additional water is added in the 2nd acid catalysed step, hydrolysis and condensation reactions proceed at similar rates. Thus newly hydrolysed molecules attach to pre-existing polymeric species. The high pressure and high temperature conditions produced during supercritical drying accelerates these condensation reactions.

In addition, the Ti-complex, which is added after partial hydrolysis of the TEOS, is expected to catalyse silanol condensation as has been previously reported [17]. Accordingly, a large number of polymeric silanol species rather than monomeric silanol groups are present. Therefore the Ti-complex and additional water in the TEOS-based system produce significantly larger particles and interstitial pores during supercritical drying than in the TMOS-based system.

On the other hand, the hydrolysis reaction proceeds further to produce monosilicic acids in the TMOS-based acid-catalysed system. These monosilicic acids act as nucleation sites for further growth. Due to a larger number of equivalent nucleation centres, the

particles formed during supercritical drying are larger in number but smaller in size than in the TEOS-based system, and also consequently small interstitial pores. These pore structures explain the observed difference in transparency between TEOS and TMOS-based systems.

Increasing the acid catalyst content in each step results in more monosilicic acids being produced in the 1st step and also the polycondensation reactions are controlled which results in a fine texture. This in turn produces a more transparent aerogel with a finer and more homogeneous structure. However, an excess of the acid has a negative influence on the microstructure and transparency of the aerogel. This may be due to over progress in the acid-catalysed polycondensation reactions in both the wet-gel formation and supercritical drying stages.

5. Conclusion

It is important to control the gelation profile during supercritical drying, because the properties of the final aerogel significantly depend on the reactions which accelerate hydrolysis and condensation at high temperature and pressures. Initial sol parameters, such as the precursors for the silicon alkoxide, catalyst, and water content, significantly influenced the pore structure and optical transparency of the final aerogel. A series of microstructures, from macroporosity to mesoporosity, could be obtained by varying the initial sol parameters.

From a catalytic viewpoint, strong acidic conditions produced a fine textured and transparent aerogel. Furthermore the TMOS-based system exhibited a better transparency and finer microstructure than the TEOS-based system. The successful control of the hydrolysis reaction in the hydrolysis step and the condensation reaction during supercritical drying, produced a very clear and transparent TiO_2 - SiO_2 binary aerogel.

References

1. R. D. SHOUP, *J. Sol-Gel Sci. Tech.* **2** (1994) 861.
2. T. M. CHE, J. B. CALDWELL and R. M. MININNI, in "Sol-gel optics" (SPIE Vol. 1328), edited by J. D. Mackenzie and D. R. Ulrich (SPIE, Bellingham WA, 1990) p. 145.
3. J. J. CALVINO, M. A. CAUQUI and J. A. PEREZ, in "Better ceramics through chemistry VI", edited by A. K. Cheetham, C. J. Brinker, M. L. Macartney and C. Sanchez (Materials Research Society, Pittsburgh, PA, 1994) p.685.
4. A. R. COOPER, in "Better ceramics through chemistry II", edited by C. J. Brinker, D. E. Clark and D. R. Ulrich (Materials Research Society, Pittsburgh, PA, 1986) p. 421.
5. B. E. YOLDAS, *J. Non-Cryst. Solids* **38, 39** (1980) 81.
6. J. ZARZYCKI, M. PRASSAS and J. PHALIPPOU, *J. Mater. Sci.* **17** (1982) 3371.
7. J. FRICKE and A. EMMERLING, *J. Amer. Ceram. Soc.* **75** (1992) 2027.
8. G. COGLIATI, M. GUGLIELMI, T. M. CHE and T. J. CLARK, in "Better ceramics through chemistry IV", edited by C. J. Brinker, D. E. Clark and D. R. Ulrich (Materials Research Society, Pittsburgh, PA, 1990) p. 329.
9. M. BEGHI, P. CHIURLO, L. COSTA, M. PALLADINO and M. F. PIRINI, *J. Non-Cryst. Solids* **145** (1992) 175.
10. S. LOWELL and J. E. SHIELDS, "Powder surface area and porosity", 2nd Edn. (Chapman and Hall, New York, 1984).

11. J. FRICKE and G. REICHENAUER, in "Better ceramics through chemistry II", edited by C. J. Brinker, D. E. Clark and D. R. Ulrich (Materials Research Society, Pittsburgh, PA, 1986) p. 775.
12. S. BRUNAUER, L. S. DEMING, W. S. DEMING and E. TELLER, *J. Amer. Chem. Soc.* **62** (1940) 1723.
13. S. J. GREGG and K. S. W. SING, in "Adsorption, surface area and porosity", 2nd Edn. (Academic Press, 1982) p. 287.
14. C. PIERCE, *J. Phys. Chem.* **57** (1953) 149.
15. J. LIVAGE, in "Better ceramics through chemistry II", edited by C. J. Brinker, D. E. Clark and D. R. Ulrich (Materials Research Society, Pittsburgh, PA, 1986) p. 717.
16. C. J. BRINKER and G. W. SCHERER, "Sol-gel science: the physics and chemistry of sol-gel processing", (Academic Press, San Diego, 1990) p. 212.
17. J. D. BASIL and CHIA-CHENG LIN, in "Ultrastructure processing of advanced ceramics", edited by J. D. Mackenzie and D. R. Ulrich (Wiley-Interscience, New York, 1988) p. 783.

*Received 10 August 1995
and accepted 13 November 1996*